Princeton Plasma Physics Laboratory

PPPL- 4526

PPPL- 4526

High-throughput Accurate-wavelength Lens-based Visible Spectrometer

Ronald E. Bell and Filippo Scotti

June, 2010

Prepared for the U.S. Department of Energy under Contract DE-AC02-09CH11466.

Princeton Plasma Physics Laboratory
Report Disclaimers

Full Legal Disclaimer

Trademark Disclaimer

PPPL Report Availability

Princeton Plasma Physics Laboratory:

http://www.pppl.gov/techreports.cfm

Office of Scientific and Technical Information (OSTI):

http://www.osti.gov/bridge

Related Links:

U.S. Department of Energy

Office of Scientific and Technical Information

Fusion Links

High-throughput accurate-wavelength lens-based visible spectrometer[a)]

Ronald E. Bell[b)] and Filippo Scotti

Princeton Plasma Physics Laboratory, Princeton, New Jersey 08543, USA

A scanning visible spectrometer has been prototyped to complement fixed-wavelength transmission grating spectrometers for charge exchange recombination spectroscopy. Fast *f*/1.8 200 mm commercial lenses are used with a large 2160 mm^{-1} grating for high throughput. A stepping-motor controlled sine drive positions the grating, which is mounted on a precision rotary table. A high-resolution optical encoder on the grating stage allows the grating angle to be measured with an absolute accuracy of 0.075 arcsec, corresponding to a wavelength error ≤ 0.005 Å. At this precision, changes in grating groove density due to thermal expansion and variations in the refractive index of air are important. An automated calibration procedure determines all relevant spectrometer parameters to high accuracy. Changes in bulk grating temperature, atmospheric temperature and pressure are monitored between the time of calibration and the time of measurement to insure a persistent wavelength calibration.

I. INTRODUCTION

Charge exchange recombination spectroscopy is a powerful technique to determine plasma temperature and plasma velocity by measuring Doppler broadening and wavelength shift of impurity ion emission. A popular spectrometer for this purpose has long been the Czerny-Turner[1] configuration with focal ratios between *f*/4.7 and *f*/12. The ability to scan in wavelength by rotating the grating makes it a flexible tool for spectroscopy. Aberrations such as astigmatism and coma arising from off-axis imaging are also features of this configuration. Recently, transmission-grating spectrometers[2] have been more widely used for this purpose. The latter have distinct advantages in higher throughput (*f*/1.8) and stigmatic imaging, which can greatly increase the number of spectra that can be placed on a detector. The transmission grating spectrometers are fixed wavelength instruments. The combination of fixed wavelength and many spectra placed on a single detector provides excellent relative wavelength stability. A combination of the best features of both of these systems (scanning, high-throughput, stigmatic imaging, wavelength stability) would be useful in a single spectroscopic diagnostic or as a complementary instrument to either improve performance or flexibility.

A prototype spectrometer has been designed to fill this gap allowing measurements at all visible wavelengths, while retaining high throughput, stigmatic imaging, and wavelength stability available on a transmission grating spectrometer. A lens-based design is used to retain the throughput and stigmatic imaging, but insuring wavelength stability requires considerably more effort. Commercial scanning spectrometers typically have a wavelength reproducibility of ~1 Å. A wavelength calibration is required each time the grating is rotated to a new position, so that the rest wavelength of a line is known to a sufficient accuracy to obtain the correct wavelength shift, *i.e.* the plasma velocity. This wavelength calibration can be accomplished by dedicating some input fibers to a calibration lamp, when suitable calibration lines are available nearby. Another option is an automated recalibration system operated between plasma discharges.[3] The ability to reliably determine the grating position to a sufficient accuracy for plasma flow measurements without recalibration would be advantageous. One goal of the spectrometer presented here is to be able to determine the absolute wavelength to an accuracy that is equal to or less than the uncertainty in the position of the fitted line over visible wavelengths even with grating motion. This would be of benefit to a velocity measurement and for line identification in more routine spectroscopy.

II. DESIGN CONSIDERATIONS

The wavelength shift, $\Delta\lambda$, corresponding to a plasma velocity, v, is given by $\Delta\lambda = \lambda v/c$, where λ is the wavelength and c is the speed of light. The accuracy needed for a plasma velocity measurement varies from ≤ 1 km/s (≤ 0.018 Å at 5291 Å) for a poloidal velocity measurement to 5-10 km/s (0.088 - 0.176 Å) for a toroidal velocity measurement. On the National Spherical Torus Experiment (NSTX), the statistical error in toroidal velocity measurement, under good conditions, is ~0.3 km/s (~0.005 Å). Reproducibly determining wavelength to this accuracy after each grating movement is a challenging though suitable criterion for the wavelength accuracy of a scanning spectrometer.

The spectrometers used for charge exchange recombination spectroscopy on NSTX are Holospec™ transmission grating spectrometers made by Kaiser Optical Systems with high dispersion gratings.[2] The parameters of these instruments, (throughput, dispersion, instrumental width) served as a benchmark for the scanning spectrometer design, along with the requirement of wavelength accuracy specified above. The custom Holospec™ on NSTX uses a commercial 85 mm, *f*/1.8 lens as collimating optics and a 58 mm *f*/1.2 lens as focusing optics. The reciprocal linear dispersion at 5291 Å is about 17.5 Å/mm. The gratings are designed for the C VI line at 5291 Å and are about 80% efficient. A 100 μm wide slit is used which corresponds to an instrumental width of about 1 Å.

[a)]Contributed paper published as part of the Proceedings of the 18th Topical Conference on High-Temperature Plasma Diagnostics, Wildwood, New Jersey, May, 2010.

[b)]Author to whom correspondence should be addressed. Electronic mail: rbell@pppl.gov.

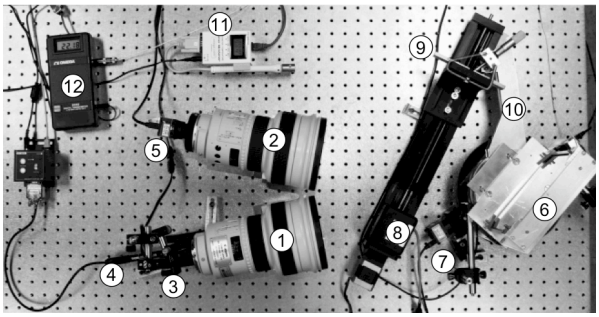

Fig. 1. The layout of the prototype spectrometer. Components include (1) collimating lens, (2) focusing lens, (3) entrance slit, (4) motorized translation stage, (5) camera, (6) grating mounted on rotary stage, (7) encoder disk and camera, (8) stepping-motor controlled slide, (9) pusher plate, (10) tangent arm, (11) barometer/thermometer, (12) thermistor/thermometer for grating temperature.

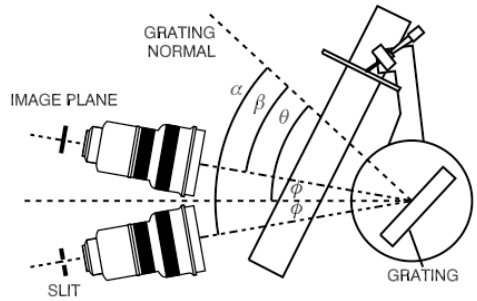

Fig 2. Schematic of spectrometer defining angles.

A prototype spectrometer was constructed using lens-based optics, a reflection grating on a rotating stage with grating angle adjusted by a sine drive.[4] (See Fig. 1.) Using Canon 200 mm *f*/1.8 EF lenses retains the stigmatic imaging and high throughput found on the transmission grating spectrometer. The clear aperture of the Canon lens is 110 mm, so a large grating was required. A 128 × 154 mm plane ruled grating on a BK7 glass substrate blazed at 5000 Å with a groove frequency of 2160 mm^{-1} and a grating efficiency about 50% for unpolarized light was obtained from Newport Corporation. A precision rotary table with an axial accuracy of 0.51 μm was obtained from ABTech Inc. to support the grating. A 25.4 cm tangent arm attached to the rotary stage is attached to a pusher plate mounted on a linear slide. The stepping-motor-controlled linear slide has a 31.7 cm travel range, 400 steps per revolution, and advances 1.58 μ per step. A precision encoder disk with a radius of 100 mm is mounted on the grating stage, allowing measurements of grating angle independent of any uncertainty in the position of the sine drive due to inherent resolution, backlash, or thermal expansion. The grating is positioned to an approximate position with the sine drive, and its position is then determined to high accuracy using the attached encoder.

A. Grating Equation

The grating equation is given by

$$\lambda_{air} = \frac{\lambda_{vac}}{n} = \frac{d}{m}\cos\gamma\left(\sin\alpha + \sin\beta\right), \quad (1)$$

where λ_{air} is the wavelength in air, λ_{vac} is the vacuum wavelength, n is the index of refraction of air, d is the groove spacing, m is the spectral order, α is the angle of incidence, β is the angle of diffraction and γ is the vertical angle with respect to the optical axis. (See Fig. 2) The vertical angle is given by $tan\gamma = y_1/f_1 = y_2/f_2$, where y_1 and y_2 are the vertical distances from the optical axis at the slit and on the detector, respectively. Let $\alpha = \alpha_0 + \tan^{-1}(x_1/f_1)$, where α_0 is the nominal angle at the entrance slit, x_1 is the horizontal displacement from the optical axis at the entrance slit and f_1 is the focal length on the collimating lens. Also let $\beta = \beta_0 + \tan^{-1}(x_2/f_2)$, where β_0 is the diffraction angle at the center of the detector, and x_2 is the horizontal distance from the detector center, and f_2 is the focal length of the focusing lens. The grating equation can then be rewritten as,

$$\lambda_{vac} = \frac{dn}{m}\cos\gamma\left(2\cos\phi\,\sin\theta + \frac{x_1}{f_1}\cos(\theta+\phi) + \frac{x_2}{f_2}\cos(\theta-\phi) - \frac{x_1^2}{2f_1^2}\sin(\theta+\phi) - \frac{x_2^2}{2f_2^2}\sin(\theta-\phi)\right), \quad (2)$$

where the grating angle $\theta=\beta_0+\phi=\alpha_0-\phi$, is the angle between the grating normal and the line bisecting the two lenses, and $2\phi=\alpha_0-\beta_0$ is the angle between the two lenses, as shown in Fig. 2. Terms above order x^2/f^2 are neglected.

From Eq. 2, the maximum wavelength of the spectrometer in first order, $m = 1$, is $2dcos\phi$. Decreasing the angle ϕ increases the wavelength range that can be reached for a given grating. An angle of $2\phi = 20°$ was chosen for the prototype spectrometer to allow spectral coverage up to ~8000Å. The grating angle variation from 3000-8000 Å is $20° < \theta < 60°$. The sine drive is configured to include travel to the zero order position, $\theta = 0°$, to aid in alignment of the spectrometer.

The reciprocal linear dispersion is given as,

$$\frac{\partial\lambda_{vac}}{\partial x_2} = \frac{dn}{mf_2}\cos\gamma\left[\cos(\theta-\phi) - \frac{x_2}{f_2}\sin(\theta-\phi)\right]. \quad (3)$$

The minimum instrumental width, w_I, is related to the slit width, w_{slit}, by the horizontal magnification from the grating and lenses,

$$w_I = \frac{\partial x_2}{\partial x_1}w_{slit} = \frac{\partial\lambda_{vac}}{\partial x_2}\frac{\partial x_1}{\partial\lambda_{vac}}w_{slit} = \frac{f_2}{f_1}\frac{\cos(\theta-\phi)}{\cos(\theta+\phi)}w_{slit}, \quad (4)$$

on the optical axis, *i.e.* $x_1=x_2=0$. The dispersion and the instrumental line width are shown in Fig. 3. The image of a spectral line will have a parabolic shape given by,

$$\Delta x_2 = \frac{m\lambda_{vac}}{2dnf_2\cos(\theta-\phi)}y_2^2, \quad (5)$$

where Δx_2 is the horizontal displacement of the image from the value at $y_2 = 0$.

B. Wavelength Accuracy and Precision Encoder

The accuracy needed for the determination of the grating angle can be computed using Eqs. 2,3 along with the desired constraint on the velocity error,

$$\Delta\theta \le \frac{\Delta v}{c}\tan\theta, \quad (6)$$

which for $\theta = 20°$, and $\Delta v = 0.3$ km/s gives $\Delta\theta = 0.075$ arcsec. An encoder with 24-bit single-turn resolution is required to achieve

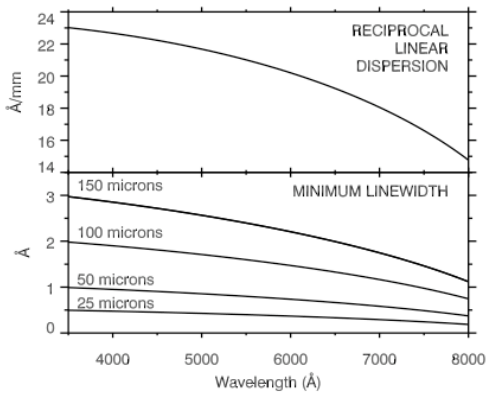

Fig. 3. Spectrometer dispersion and minimum instrumental line width vs. wavelength.

this accuracy. Single-turn commercial encoders are typically 16-bit. Using absolute rotary encoder technology patented by the NASA Goddard Space Flight Center,[5] an encoder was designed for the prototype spectrometer to the resolution required. The encoder uses pattern recognition of a sequence of bit codes arranged in a 4×4 pattern. There are 10800 code groups (~13.4 bits) and fiducial markers every 2 minutes of arc around a 100 mm radius disk. The precise centroid position of the fiducial markers is determined by fitting to a high accuracy in much the same way the centroid position of a spectral line is determined. The encoder read out is done with a pair of small USB operated CMOS cameras (752×480, 6 micron pixels) with illumination by LEDs. Two cameras placed precisely 180° apart allow the encoder angle to be determined to a high accuracy, canceling any errors due to radial runout of the rotary table or non-concentric placement of the encoder disk.

C. Temperature and Pressure Sensitivity

The index of refraction of air is dependent on air temperature and barometric pressure,[6] so an apparent shift in wavelength can occur if there is a sufficient change in environmental conditions between the time of a wavelength calibration and the time of measurement. Also, the grating substrate can undergo thermal expansion that can change the groove density of the grating causing apparent shifts in wavelength and changes in apparent velocity. Recognizing that $n = n(T,P)$, $d = d(T)$ and taking the derivatives of the grating equation with respect to grating temperature, air temperature and air pressure,

$$\frac{\partial \lambda_{vac}}{\partial T_g} = \frac{\lambda_{vac}}{d}\frac{\partial d}{\partial T_g}, \quad \frac{\partial \lambda_{vac}}{\partial T_{air}} = \frac{\lambda_{vac}}{n}\frac{\partial n}{\partial T_{air}}, \qquad (7)$$

$$\frac{\partial \lambda_{vac}}{\partial P} = \frac{\lambda_{vac}}{n}\frac{\partial n}{\partial P}. \qquad (8)$$

Here T_g refers to the bulk grating temperature in the first part of Eq. 7, which relates thermal changes in the grating lead to a change in groove density. T_{air} refers to the air temperature and P to air pressure.

If κ is the expansion coefficient of the grating substrate material, then $\partial d/\partial T = \kappa$, so the change in wavelength due to thermal expansion of the grating is $\Delta\lambda_{vac}^{grating} = \lambda_{vac}\kappa$. The expansion coefficient for BK7 glass is $\kappa_{BK7} = 7.5\times10^{-6}$ /K, so the apparent change in velocity resulting from thermal expansion is $\Delta v = c\kappa_{BK7} = 2.25$ km/s/K. With $\Delta v = 0.3$ km/s as the requirement

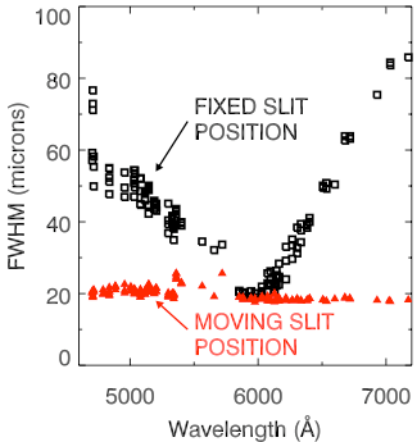

Fig. 4. (Color online) With a fixed entrance slit position, a large variation in the FWHM from chromatic aberration is measured. By adjusting the slit position along the optical axis to optimize focus, the expected FWHM of the instrumental function is recovered at all wavelengths.

for wavelength accuracy, bulk thermal changes of the grating ≥ 0.12°C are significant. To compensate for any thermal expansion, the bulk grating temperature is monitored with a precision thermistor thermometer accurate to ±0.015 °C Substituting a grating with a ZeroDur® substrate would significantly reduce this issue, since it has an expansion coefficient of 0 ± 10^{-7}/K, and a change in bulk temperature of ±10 °C could be tolerated.

The change in apparent velocity due to changes in air temperature can be estimated using the refractive index computed from the Ciddor equation[6] to determine a change in the refractive index $\Delta n = n(T+\Delta T) - n(T)$,

$$\frac{\partial v}{\partial T} = \frac{c}{n}\frac{\partial n}{\partial T} \approx \frac{c}{n}\frac{\Delta n}{\Delta T} \approx -0.29 \text{ km/s/K}. \qquad (9)$$

Similarly, apparent shifts in velocity due to air pressure changes can be estimated using $\Delta n = n(P+\Delta P) - n(P)$,

$$\frac{\partial v}{\partial P} = \frac{c}{n}\frac{\partial n}{\partial P} \approx \frac{c}{n}\frac{\Delta n}{\Delta P} \approx 8.2\times10^{-4} \text{ km/s/Pa} \qquad (10)$$

One atmosphere is 103125 Pa, so a 1% change in air pressure will result in an apparent change in velocity of ~0.8 km/s. Changes in air pressure and temperature are monitored with a computer controlled thermometer (± 0.1°C) and barometer (± 200 Pa) between the time of calibration and the time of measurement, so that changes in atmospheric conditions can be included in the determination of absolute wavelength. Note that although relative humidity will also affect the index of refraction of air, it is neglected here, since for a 0% to 100% change in relative humidity, the effect on velocity are less than 0.2 km/s.

D. Chromatic Aberration

Initial measurements of the instrumental width showed a wide variation (factor of four) versus wavelength, in contrast to predictions from Eq. 4. For example, when focused at a particular wavelength, lines to the red and blue suffered from larger instrumental widths. The reason for the discrepancy was determined to be the chromatic aberration of the Canon lenses. To compensate for the change the focal length with wavelength, a motorized linear translation stage was added to move the entrance slit along the optical axis. The position of optimum

focus over a range of wavelengths was determined by scanning the translation stage until the observed FWHM was minimized. A 2 mm range of motion was required to adjust the focus of reference calibration lines over the visible spectrum. With this adjustment, the expected instrumental width was recovered for all wavelengths, see Fig. 4.

III. ALIGNMENT AND CALIBRATION

A high precision measurement of the grating angle is not sufficient to insure the required wavelength accuracy. All of the parameters in the grating equation must be fit to a sufficient accuracy as well. To the extent that a parameter cannot be aligned to sufficient accuracy, it must be determined, *i.e.* fitted, during the calibration process. For example, the normal to the detector may not be aligned with the optical axis. The tilt of the detector about a vertical axis, though small, will change the apparent distance from the detector center. In the horizontal plane,

$$\frac{x_2}{f_2} = \frac{w_{pixel}(p - p_0)\cos\varepsilon_x}{f_0 + w_{pixel}(p - p_0)\sin\varepsilon_x}, \qquad (11)$$

where p is the pixel position, p_0 is the position on the optical axis, w_{pixel} is the width of a pixel, ε_x is the horizontal tilt of the detector, and f_0 is the nominal focal length of the lens. Tilt about a horizontal axis, ε_y, must also be considered,

$$\frac{y_2}{f_2} = \frac{w_{pixel}(l - l_0)\cos\varepsilon_y}{f_0 + w_{pixel}(l - l_0)\sin\varepsilon_y}, \qquad (12)$$

where l is the vertical line position, and l_0 is the vertical line position at the optical axis.

The addition of the translation stage for the entrance slit solved a problem with instrumental width but added an alignment issue. If the slit is not aligned with the optical axis, the angle of incidence may change with the slit movement through x_1/f_1,

$$\frac{x_1}{f_1} = \frac{s + (L - L_0)\sin\sigma}{f_0 + (L - L_0)\cos\sigma}, \qquad (13)$$

where L is the measured position of the translation stage, L_0 is a reference point at the optical axis, s is a displacement from the optical axis, and σ is the angle with respect to the optical axis. The distance $(L\text{-}L_0)\cos\sigma$ is twice the change in the focal length of the lens due to chromatic aberration. A small offset θ_0 in the grating angle associated with angular change associated with the reference point L_0 is also to be expected. Using Eq. 2, and Eqs. 11-13, the parameters ϕ, p_0, l_0, ε_x, ε_y, s, f_0, and θ_0 must be fit to sufficient accuracy to meet the requirement on the error in velocity. The angle σ can be determined using the scan of slit position to determine optimal focus by monitoring $\Delta p/\Delta L$, the ratio of the change in horizontal position of the line on the detector to the change in slit position,

$$\sin\sigma = w_{pixel}\frac{\cos(\theta + \phi)}{\cos(\theta - \phi)}\frac{f_1}{f_2}\frac{\Delta p}{\Delta L}. \qquad (14)$$

It is assumed that a careful alignment procedure has aligned the grating and removed any rotation of the detector about its normal. Full details of the alignment and calibration procedure are described elsewhere.[7]

IV. RESULTS

The parameters predicted for this spectrometer were confirmed during the testing, e.g. the dispersion, image curvature and instrumental width after adopting the adjustable entrance slit position. All components of the system, including the stepping motor, the encoder cameras, and the image plane camera, the slit translation stage, the thermometers and barometer were all computer controlled using Visual Basic software. The determination of line position to the necessary accuracy was somewhat hampered by the detector used for testing the spectrometer, *i.e.* a 1280×1024 CMOS camera with 5.2 micron pixels and 8-bit digitization, similar to the cameras used for reading the encoder position. The readout noise and the limited available integration time limited the accuracy of the line position measurement. Using multiple exposures and the full height of the detector allowed the necessary accuracy. Fitting the spectrometer parameters using the unblended neon lines at wavelength from 5800-7250 Å, allowed an excellent fit to the spectrometer parameters with a residual error from the fit of Δv = 0.2 km/s, less than the goal of 0.3 km/s. These residual were only a few milli-Ångstroms. The computed error for the fitted wavelength based on computed errors in the fitted parameters were much lower, assuming random errors. The testing also showed that a good alignment was necessary to achieve these results. The error in repositioning the grating was demonstrated to be better than the expected error in the fitted line position.

A comparison can be made between this spectrometer with the transmission grating spectrometers now in use on NSTX for charge exchange recombination spectroscopy. The dispersion at the C VI wavelength of 5291 Å is 21.3 Å/mm compared 17.5 Å/mm for the transmission grating spectrometer. For an instrumental width of 1 Å, the prototype spectrometer needs a 61 μm slit compared to a 100 μm slit for the transmission grating spectrometer. The grating transmission for unpolarized light also favors the transmission grating by 80% to about 50% for the reflection grating. Overall, the throughput of the prototype spectrometer is about 38% of the transmission grating spectrometer.

ACKNOWLEDGEMENTS

The authors would like to acknowledge the help of W. Boeglin who designed the grating rotation stage. The support and encouragement of D. W. Johnson and B. C. Stratton is also appreciated. This work was supported by the U. S. Dept. of Energy, Contract No. DE-AC02-09CH11466.

REFERENCES

[1] M. Czerny and A. F. Turner, Z. Phys. **61**, 792 (1930).
[2] R. E. Bell, Rev. Sci. Instrum. **75**, 4158 (2004).
[3] P. Gohil, K. H. Burrell, R. J. Groebner, K. Holtrop, D. H. Kaplan, P. Monier-Garbet, Rev. Sci. Instrum. 70, 878 (1999).
[4] D. L. Dimock, J. Opt. Soc. Am. 50, 819 (1960).
[5] D. B. Leviton, U.S. Patent No. 5,965,879 (12 October 1999).
[6] P. E. Ciddor, Appl. Opt. 35, 1566 (1996).
[7] F. Scotti and R. E. Bell, "High accuracy wavelength calibration for a scanning visible spectrometer", these conference proceedings.

The Princeton Plasma Physics Laboratory is operated
by Princeton University under contract
with the U.S. Department of Energy.

Information Services
Princeton Plasma Physics Laboratory
P.O. Box 451
Princeton, NJ 08543

Phone: 609-243-2750
Fax: 609-243-2751
e-mail: pppl_info@pppl.gov
Internet Address: http://www.pppl.gov